



# Post-glacial flooding of the Bering Land Bridge dated to 11 cal ka BP based on new geophysical and sediment records

Martin Jakobsson<sup>1</sup>, Christof Pearce<sup>1,2</sup>, Thomas M. Cronin<sup>3</sup>, Jan Backman<sup>1</sup>, Leif G. Anderson<sup>4</sup>, Natalia Barrientos<sup>1</sup>, Göran Björk<sup>4</sup>, Helen Coxall<sup>1</sup>, Agatha de Boer<sup>1</sup>, Larry A. Mayer<sup>5</sup>, Carl-Magnus Mörrth<sup>1</sup>, Johan Nilsson<sup>6</sup>, Jayne E. Rattray<sup>1</sup>, Christian Stranne<sup>1,5</sup>, Igor Semiletov<sup>7,8</sup>, and Matt O'Regan<sup>1</sup>

<sup>1</sup>Department of Geological Sciences and Bolin Centre for Climate Research, Stockholm University, 10691 Stockholm, Sweden

<sup>2</sup>Department of Geoscience, Aarhus University, 8000 Aarhus, Denmark

<sup>3</sup>US Geological Survey MS926A, Reston, Virginia 20192, USA

<sup>4</sup>Department of Marine Sciences, University of Gothenburg, 412 96 Gothenburg, Sweden

<sup>5</sup>Center for Coastal and Ocean Mapping, University of New Hampshire, Durham, New Hampshire 03824, USA

<sup>6</sup>Department of Meteorology, Stockholm University, 106 91 Stockholm, Sweden

<sup>7</sup>Pacific Oceanological Institute, Far Eastern Branch of the Russian Academy of Sciences, 690041 Vladivostok, Russia

<sup>8</sup>Tomsk Polytechnic University, Tomsk, Russia

*Correspondence to:* Martin Jakobsson (martin.jakobsson@geo.su.se)

Received: 26 January 2017 – Discussion started: 13 February 2017

Accepted: 1 July 2017 – Published: 1 August 2017

**Abstract.** The Bering Strait connects the Arctic and Pacific oceans and separates the North American and Asian landmasses. The presently shallow ( $\sim 53$  m) strait was exposed during the sea level lowstand of the last glacial period, which permitted human migration across a land bridge today referred to as the Bering Land Bridge. Proxy studies (stable isotope composition of foraminifera, whale migration into the Arctic Ocean, mollusc and insect fossils and paleobotanical data) have suggested a range of ages for the Bering Strait reopening, mainly falling within the Younger Dryas stadial (12.9–11.7 cal ka BP). Here we provide new information on the deglacial and post-glacial evolution of the Arctic–Pacific connection through the Bering Strait based on analyses of geological and geophysical data from Herald Canyon, located north of the Bering Strait on the Chukchi Sea shelf region in the western Arctic Ocean. Our results suggest an initial opening at about 11 cal ka BP in the earliest Holocene, which is later than in several previous studies. Our key evidence is based on a well-dated core from Herald Canyon, in which a shift from a near-shore environment to a Pacific-influenced open marine setting at around 11 cal ka BP is observed. The shift corresponds to meltwater pulse 1b (MWP1b) and is interpreted to signify relatively rapid breaching of the Bering

Strait and the submergence of the large Bering Land Bridge. Although the precise rates of sea level rise cannot be quantified, our new results suggest that the late deglacial sea level rise was rapid and occurred after the end of the Younger Dryas stadial.

## 1 Introduction

The  $\sim 85$  km wide and  $\sim 53$  m deep Bering Strait forms a Pacific–Arctic connection that influences Arctic Ocean circulation, surface water composition, nutrient flux, sea ice and marine ecosystems (Grebmeier, 2011; Watanabe and Hasumi, 2009). On average, approximately 1.1 Sv of relatively fresh and nutrient-rich water is presently flowing into the Arctic Ocean from the Pacific (Woodgate et al., 2015). The throughflow was initially proposed to be primarily driven by the mean sea level difference between the Pacific (higher) and the Arctic Ocean (lower; Stigebrandt, 1984), although later work has pointed to the importance of both the far-field wind stress (De Boer and Nof, 2004a, b; Ortiz et al., 2012) and the near-field wind stress (Aagaard et al., 2006; Danielson et al., 2014). An open Bering Strait is proposed to

dampen abrupt climate transitions, thereby emphasizing the critical role of a Pacific–Arctic connection in Earth’s climate system (De Boer and Nof, 2004b; Hu et al., 2012, 2015; Sandal and Nof, 2008).

Along with increased knowledge of Quaternary glacial–interglacial cycles and the huge effects on sea levels from the waxing and waning of ice sheets came the realization that the shallow Bering Strait region must have formed a land bridge connecting North America and northeastern Asia during glacial sea level lowstands (Hopkins, 1967; Hultén, 1937; McManus and Creager, 1984). In honor of Vitus Bering, who entered the strait in 1728, Swedish botanist Eric Hultén referred to the shallow area between Alaska and Chukotka as Beringia in a study suggesting that this area was once sub-aerial and formed a tundra plain (Hultén, 1937). The term Beringia was later used to include the entire stretch from the MacKenzie River in Canada to the Kolyma River in north-eastern Siberia. Here we use the term Bering Land Bridge for the specific subaerial connection that formed during a lower sea level and permitted the crossing of the Bering Strait by foot.

The precise timing of the latest flooding of the Bering Land Bridge and the reestablishment of a marine connection between the Pacific and Arctic oceans following the last glaciation has been difficult to establish. Published estimates based on minimum and maximum age constraints for the flooding event place the opening somewhere between about 10 300 and 13 100 cal yr BP (Dyke and Savelle, 2001; Elias et al., 1992, 1996; England and Furze, 2008; Keigwin et al., 2006). Evidence for the flooding of the Bering Strait includes the first occurrence of the Pacific mollusc species *Cyrtodaria kurriana* in the western Canadian Arctic Archipelago (England and Furze, 2008), the dating of peat in the Chukchi Sea (Elias et al., 1992, 1996), an abrupt change in  $\delta^{18}\text{O}$  of foraminifera toward lighter values along with a change toward heavier values in  $\delta^{13}\text{C}$ , a change toward smaller grain size values in a sediment core from Hope Valley in the eastern Chukchi Sea (Keigwin et al., 2006) and the first occurrence of bowhead whales in the western Canadian Arctic Archipelago after the last glaciation (Dyke and Savelle, 2001).

The exact age of the flooding event is important as it both ends the last period of easy human and animal migration between North America and northeastern Asia (Goebel et al., 2008) and affects the Arctic Ocean circulation, stratification and sea ice (Woodgate et al., 2012, 2015), and potentially the global climate stability (De Boer and Nof, 2004b). The bathymetry of the Bering Strait region, as portrayed by the Alaska Region Digital Elevation Model (ARDEM; Danielson et al., 2015), shows that the shallowest sill between the Pacific Ocean and Arctic Ocean is not located directly in the presently  $\sim 53$  m deep Bering Strait (Fig. 1). Rather, there are two slightly shallower sills located to the north and the south of the strait, both  $\sim 47$  m deep today. However, isostatic changes and other tectonic movements as well as sedi-

ment deposition and erosion after deglaciation add uncertainties as to which of the sills acted as the final critical barrier separating the Pacific and Arctic oceans. Placing published timings of the breaching of the Bering Land Bridge in global eustatic sea level reconstructions (Fairbanks, 1989; Lambeck et al., 2014) indicates that either the local relative sea level history was different from the global eustatic sea level due to local isostatic adjustments of the Bering Land Bridge area or that the proposed chronologies were incorrect (Fig. 2).

To better establish the timing of the Bering Strait opening, we analyzed new geophysical mapping data and sediment cores from Herald Canyon, located immediately north of the modern strait. These data, acquired during the SWERUS-C3 (Swedish–Russian–US Arctic Ocean Investigation of Climate–Cryosphere–Carbon Interactions) 2014 expedition with the Swedish icebreaker (IB) *Oden*, provide new insights about the onset of Pacific water influx into the Arctic Ocean. The studied sediment cores are well dated, permitting precise determination of when the Arctic Ocean became connected to the Pacific Ocean after the last glacial period.

## 2 Methods

### 2.1 Expedition

The SWERUS-C3 2014 expedition on IB *Oden* consisted of two 45-day legs in 2014. The geophysical mapping data and sediment cores from Herald Canyon presented in this work were collected during leg 2, which departed on 21 August from Barrow, Alaska and ended on 3 October in Tromsø, Norway. Herald Canyon was the first survey area during leg 2. Four transects across the canyon were completed, here referred to as transects 1–4 (Fig. 1b). We mainly show data from the northern part of Herald Canyon (transects 3 and 4) where the two piston cores SWERUS-L2-2-PC1 and SWERUS-L2-4-PC1 were retrieved, hereafter referred to as 2-PC1 and 4-PC1, respectively. These cores provide a detailed record of the late- to post-glacial paleoceanography and new insights into the flooding history of the Bering Land Bridge.

### 2.2 Geophysical mapping

IB *Oden* is equipped with a hull-mounted Kongsberg EM 122 (12 kHz;  $1^\circ \times 1^\circ$ ) multibeam echosounder and integrated SBP 120 (2–7 kHz;  $3^\circ \times 3^\circ$ ) chirp sonar. The multibeam chirp system has a Seatex Seapath 330 unit for the integration of GPS navigation, heading and attitude. The multibeam and chirp sonar were both in continuous operation during leg 2, and the chirp sonar used a 2.5–7 kHz chirp pulse. Temperature and salinity data from CTD (conductivity, temperature, depth) stations were used to calculate sound speed profiles for the calibration of the multibeam. These were supplemented with regular XBT (expendable bathythermograph) casts from which temperature alone was used to estimate the

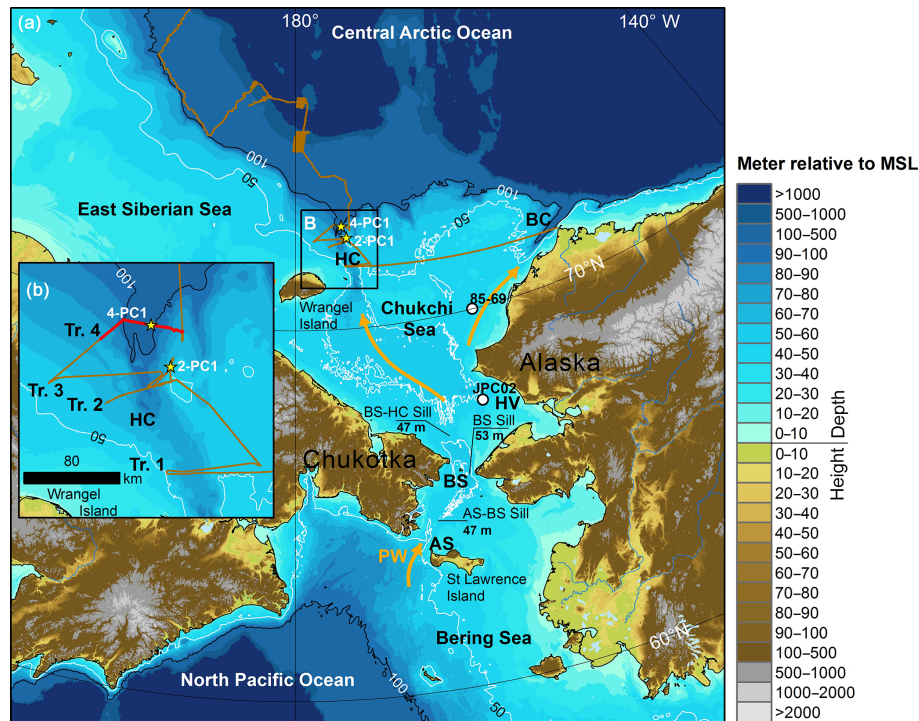


**Figure 1.** (a) Overview map of the western Arctic Ocean and the northern Pacific Ocean connected by the  $\sim 53$  m deep Bering Strait (BS). The study area of Herald Canyon (HC) is shown in detail in the inset map (b). The main route for the present Pacific water (PW) inflow into the Arctic Ocean through the BS is shown with orange arrows. There are two bathymetric sills slightly shallower ( $\sim 47$  m deep) than the BS, the BS-HC sill and the Anadyr Strait (AS)-BS sill. The locations of SWERUS-C3 cores 4-PC1 and 2-PC1, the focus of this study, are shown with yellow stars. Key cores from previous studies referred to in this work regarding the reopening of the BS after the LGM are shown with white dots (85–69, Elias et al., 1992, 1996; JPC 02, Keigwin et al., 2006). The bathymetry is from the Alaska Region Digital Elevation Model (ARDEM; Danielson et al., 2015). The leg 2 cruise track of the SWERUS-C3 expedition in 2014 is shown with a brown line. HV = Hope Valley. Tr. 1, 2, 3 and 4 indicate the transects across Herald Canyon referred to in the text. Figure 4 shows transects 3 and 4, and Fig. 5 shows transect 4.

sound speed. Multibeam bathymetry was post-processed using a combination of Caris and Fledermaus QPS software. Regular grids with a horizontal resolution of  $15 \times 15$  m were produced in the Herald Canyon area. Here the multibeam bathymetry is mainly used to reference the chirp sonar profiles properly to seafloor depth. The chirp sonar profiles were post-processed and interpreted in the open-source software OpendTect created by dGB Earth Sciences.

### 2.3 Sediment coring

Sediment cores were taken with the Stockholm University piston corer. This corer is launched with a system specifically designed for IB *Oden* and can handle up to 12 m long cores from the aft deck. The corer uses 110 and 100 mm outer and inner diameter PVC liners and was typically rigged with a core head weighing 1360 kg during the SWERUS-C3 expedition. The trigger weight of the piston corer consists of a 1 m long gravity corer. The 8.2 m long core 2-PC1 was retrieved in 57 m of water depth at  $175^{\circ}19.2' \text{ W}$ ,  $72^{\circ}30.0' \text{ N}$ . The 6.1 m long core 4-PC1 was retrieved from 120 m of water depth at

$175^{\circ}43.6' \text{ W}$ ,  $72^{\circ}50.3' \text{ N}$  (Fig. 1). The trigger core of 2-PC1 was empty, while the trigger core of 4-PC1 recovered 46 cm. Both 2-PC1 and 4-PC1 are from the eastern side of Herald Canyon.

### 2.4 Measured sediment physical and chemical properties

High-resolution (1 cm) shipboard measurements of sediment physical properties, including bulk density, magnetic susceptibility and p-wave velocity, were performed using a Geotek Multi-Sensor Core Logger (MSCL; Fig. 3). The cores were logged before being split, visually described with respect to lithology and sedimentological structures and then sampled for additional analyses. Shear strength measurements were performed on the split cores prior to sampling using a fall cone device. Biogenic silica (BSi) was measured on 10 evenly spaced samples from core 4-PC1, following the wet alkaline extraction technique to measure BSi from Conley and Schelske (2002). Approximately 30 mg of freeze-dried and homogenized sediment from each sample was ex-

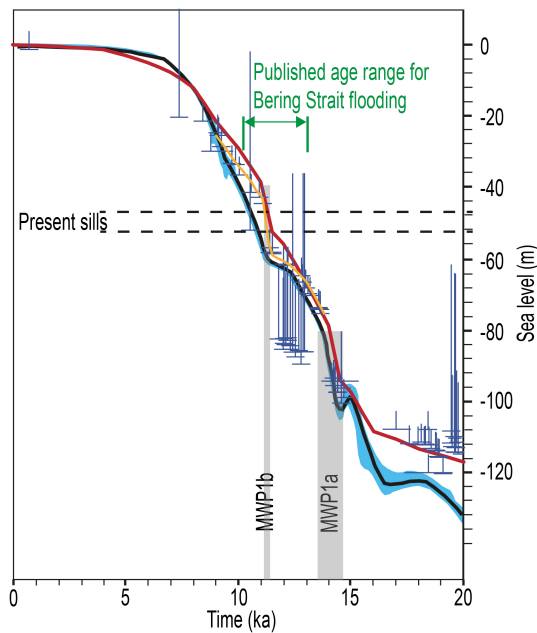


**Figure 2.** Different estimations of eustatic sea level change over the last 20 000 years. The black curve shows the ice-volume-equivalent sea level change along with its 95 % probability limit in blue by Lambeck et al. (2014). The blue bars show sea level estimations using the coral reef record at Barbados, and the red line is the prediction of the sea level history using the ICE-5G (VM2) model at the same site (Peltier and Fairbanks, 2006). The orange line is the most recent reconstruction using the Barbados coral reefs by Abdul et al. (2016). The time intervals of meltwater pulse 1a (MWP1a) and meltwater pulse 1b (MWP1b) are indicated by the gray bars. The depths of the present sills in the Bering Strait area (see Fig. 1) are shown by black stippled lines.

tracted and placed in an alkaline solution (1 %  $\text{Na}_2\text{CO}_3$ ) at 85°C. After 3, 4 and 5 h of leaching, aliquots were taken and measured for dissolved Si using a Thermo iCAP 6500 Duo ICP-OES (inductively coupled plasma optical emission spectroscopy). The BSi is dissolved first, implying that the measurements made on aliquots taken after 3, 4 and 5 h include Si from minerals. A curve is constructed from all measurements and the BSi concentration is estimated from the point at which the curve intercepts zero time. While the estimated uncertainty is as high as  $\pm 20\%$ , the method has been shown to be reproducible and capable of providing trends in sediment BSi variations through interlaboratory comparison studies (Conley, 1998). Stable carbon isotopes of bulk organic matter were measured every 10 cm in both cores 2-PC1 and 4-PC1. Samples were freeze-dried, homogenized and treated with an HCl solution to remove carbonate; approximately 10 mg was folded into small tin cups. Based on standard measurement, the error in  $\delta^{13}\text{C}_{\text{org}}$  values was better than  $\pm 0.1\%$ . The  $\delta^{13}\text{C}_{\text{org}}$  values were obtained with a Finnigan DeltaV Advantage mass spectrometer coupled to a Carlo Erba NC2500 elemental analyzer.

## 2.5 Dating

The chronostratigraphy of core 2-PC1 has been presented by Pearce et al. (2017). A short summary of the applied dating methods and a description of the dated material are presented here. Tephra from the 3.6 ka BP Aniakchak CFE II eruption was observed in 2-PC1 and used to constrain the Holocene  $^{14}\text{C}$  marine reservoir age in shallow areas of the Chukchi Sea. This local  $\Delta R$  (477 years) was applied during calibration of the radiocarbon ages using the Marine13 calibration curve (Reimer et al., 2013) and the OxCal 4.2 program (Ramsey, 2009). Molluscs from 14 different sediment depth levels were dated from core 2-PC1 using accelerator mass spectrometry (AMS)  $^{14}\text{C}$  measurements (Pearce et al., 2017).

In core 4-PC1, eight different levels were AMS radiocarbon dated (Table 1; see also Cronin et al., 2017). Radiocarbon ages are calibrated using the same approach as for core 2-PC1 described above. One of two dates at 417 cm depth is, however, clearly too old compared to the other radiocarbon samples (Table 1; Fig. 3b). This date is considered to have been derived from a reworked shell and therefore treated as an outlier. Based on the identified major change in the sediment physical properties and geochemical composition of core 4-PC1 (Fig. 3), two different values are used for the local marine radiocarbon reservoir correction. Below the major change at around 407 cm, we assume that there is no connection to the Pacific Ocean and thus no inflow of relatively old Pacific waters. For this lower section,  $\Delta R = 50 \pm 100$  years is applied based on present values in the Laptev Sea (Bauch et al., 2001), the closest site with modern information on the reservoir age from a shallow, coastal Arctic shelf setting with no Pacific influence (Reimer and Reimer, 2001). In the upper 400 cm of core 4-PC1, representing the late Holocene, a larger reservoir is expected due to the Pacific influence and  $\Delta R = 300 \pm 200$  years is applied to the radiocarbon dates in this section. This value is lower than the 477 years derived for neighboring core 2-PC1 (Pearce et al., 2017) because of the greater water depth at the site. The rationale behind this is that Atlantic-sourced waters are at times present on the northern Chukchi shelf and upwell into the deeper section of Herald Canyon (Pickart et al., 2010; Pisareva et al., 2015), resulting in a lower radiocarbon reservoir age.

## 3 Results

### 3.1 Herald Canyon morphology and acoustic stratigraphy

Herald Canyon topographically steers the western branch of Pacific water flowing into the Arctic Ocean (Pickart et al., 2010; Woodgate and Aagaard, 2005), implying that cores 2-PC1 and 4-PC1 are strategically placed to record this critical component of Arctic Ocean paleoceanography. Herald Canyon is well portrayed by the bathymetric gridded compilation ARDEM (Figs. 1, 4). The deepest section of the

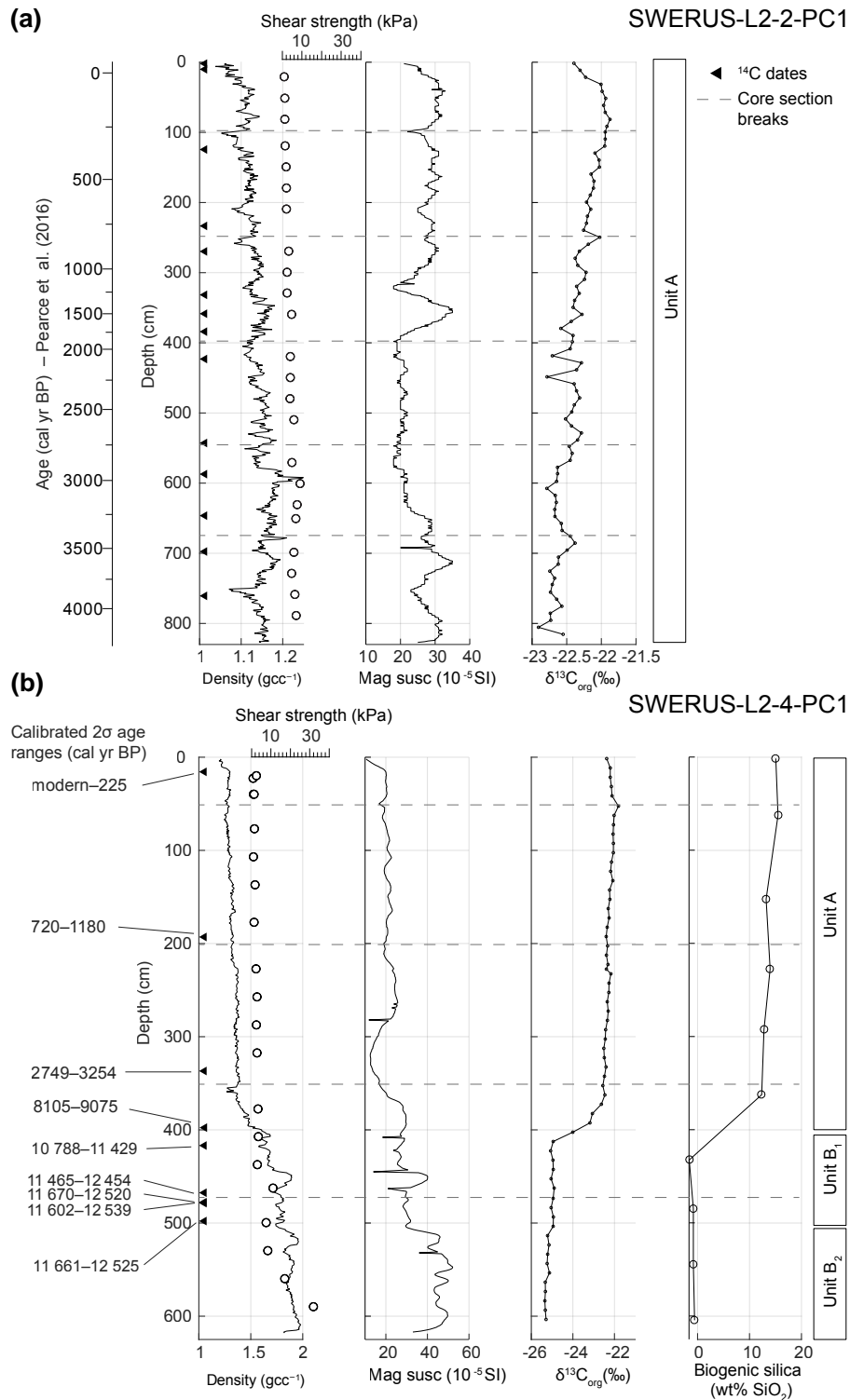


**Figure 3.** Measured physical properties (density, magnetic susceptibility and undrained shear strength) and geochemical proxy data ( $\delta^{13}C_{org}$  and biogenic silica) for cores 2-PC1 (a) and 4-PC1 (b). The black triangles on the depth axes show the positions of AMS radiocarbon dates, and the dashed lines indicate depths of the different sections of the cores. Interpreted lithologic units are shown on the right. All data are presented versus depth in the core and supplemented by an age axis for core 2-PC1 (a) based on the age–depth model presented in Pearce et al. (2017) and  $2\sigma$ -calibrated age ranges for core 4-PC1 (b); see also Table 1.

**Table 1.** AMS radiocarbon ages and calibrations for core 4-PC1 and literature dates constraining the Beringia flooding. All ages are calibrated with the Marine13 (Reimer et al., 2013) radiocarbon calibration curve, except for beta-43953 (Elias et al., 1992), which is calibrated using IntCal13 (Reimer et al., 2013).

Core/site	Reference	Depth (cm)	Material	Lab ID	$^{14}\text{C}$ age (yr BP)	$\Delta R$ (years)	1 $\sigma$ age range (cal yr BP)		2 $\sigma$ age range (cal yr BP)		median age (cal yr BP)
							from	to	from	to	
SWERUS-L2-4-PC1	This study	16	Mollusc: <i>Nuculana permula</i>	LuS11278	445 ± 35	300 ± 200	79	−64	225	−64	51
SWERUS-L2-4-PC1	This study	192.5	Mollusc: <i>Yoldia</i> sp.	LuS11279	1700 ± 35	300 ± 200	1065	820	1180	720	952
SWERUS-L2-4-PC1	This study	337	Benthic foraminifera	NOSAMS133772	3490 ± 25	300 ± 200	3129	2859	3254	2749	2998
SWERUS-L2-4-PC1	This study	417	Mollusc	NOSAMS131218	10200 ± 30	50 ± 100	11260	11020	11429	10788	11143
SWERUS-L2-4-PC1	This study	417	Mollusc	NOSAMS131219*	11400 ± 35	50 ± 100	12928	12701	13070	12635	12826
SWERUS-L2-4-PC1	This study	467	Mollusc	NOSAMS131220	10700 ± 30	50 ± 100	12236	11772	12454	11465	11994
SWERUS-L2-4-PC1	This study	479	Mollusc	NOSAMS131221	10750 ± 30	50 ± 100	12339	11900	12520	11670	12101
SWERUS-L2-4-PC1	This study	484	Mollusc: <i>Yoldia</i> sp.	LuS11280	10745 ± 55	50 ± 100	12349	11875	12539	11602	12088
SWERUS-L2-4-PC1	This study	499	Mollusc	NOSAMS131222	10750 ± 35	50 ± 100	12341	11899	12525	11661	12100
85-69	Elias et al. (1992)	90–95	Screened peat	Beta-43953	11000 ± 60	n.a.	12950	12774	13017	12728	12866
HLY0204-02JPC	Keigwin et al. (2006)	845.5	Benthic forams: <i>E. excavatum</i>	n.a.	10900 ± 140	50 ± 100	12561	12075	12702	11707	12279
Cape Baring	Dyke and Savelle (2001)	n.a.	Bowhead whale bone	TO-7755	10210 ± 70	740 ± 100	10476	10198	10645	10030	10334
Mercy Bay	England and Furze (2008)	n.a.	Mollusc: <i>Cyrtodaria kurriana</i>	TO-12496	12380 ± 110	740 ± 100	13273	12956	13390	12779	13109

\* Outlier not included in the age model of 4-PC1.

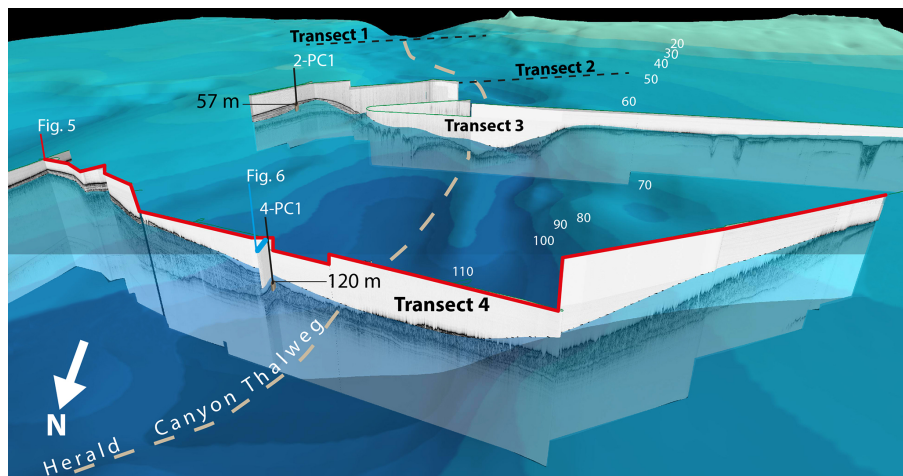


**Figure 4.** A 3-D view of the bathymetry of Herald Canyon and the chirp sonar profiles acquired along crossing transects. Locations of the coring sites are shown by black bars.

canyon valley (thalweg) reaches a depth of 120 m in ARDEM approximately 4 km south of transect 4 before it widens to lose bathymetric expression when merging with the flat shelf. Along the southernmost transect 1, closest to Wrangel Island, the thalweg has a water depth of  $\sim 71$  m. This yields a slope of about  $0.02^\circ$  over 140 km. A mismatch exists between the multibeam bathymetry and chirp profiles collected with IB *Oden* and the bathymetry of ARDEM at some locations. Of particular importance here is that transect 4, where core 4-PC is located, reaches a depth of  $\sim 120$  m and is thus slightly deeper than suggested by ARDEM, while the location of core 2-PC is  $\sim 7$  m shallower than the ARDEM depth (Figs. 4, 5). However, these depth differences must be considered relatively small since ARDEM is a gridded compilation with a cell size of  $1 \times 1$  km (Danielson et al., 2015). The collected multibeam bathymetry with IB *Oden* do not cover an area large enough to produce a new bathymetric map of Herald Canyon.

The chirp sonar profiles reveal that more sediments are accumulated along the eastern side of Herald Canyon, while the western side is characterized by a scoured, harder seafloor and substantially thinner sediment depositions (Figs. 4, 5a, b). The difference in bottom hardness was apparent when the 12 kHz multibeam sonar had problems with sub-bottom penetration in soft sediments along the eastern side. This caused the multibeam to occasionally record the depth several meters sub-bottom rather than the seafloor because the bottom-tracking algorithm did not detect a large enough acoustic impedance contrast at the soft seabed.

The lowermost defined reflector R1 marks an unconformity. Sediment accumulations in Herald Canyon that were penetrated by the chirp sonar rest on this unconformity, and there are dipping reflectors clearly visible below R1 in several of the acquired profiles (Fig. 5a, b). The sediment section above R1 on the eastern side of the deepest part of transect 4, where core 4-PC1 is located, is up to 55 ms

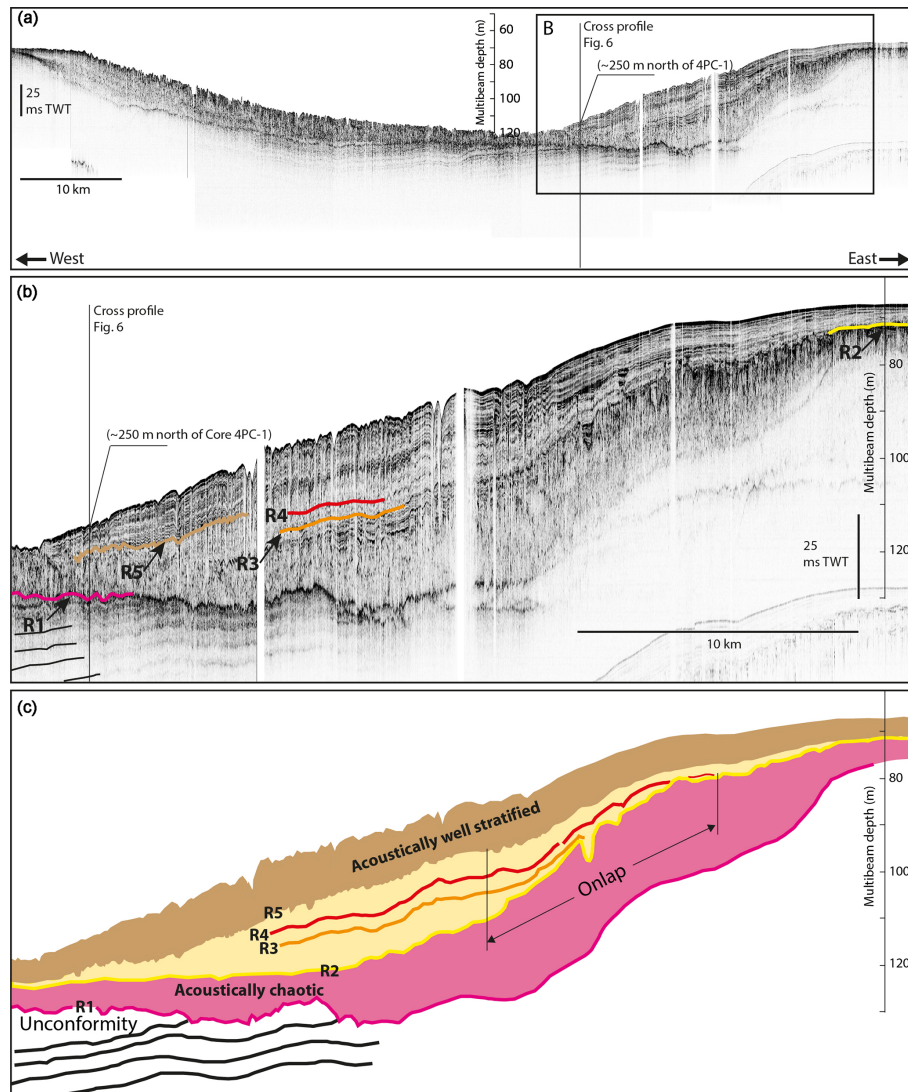


**Figure 5.** Chirp sonar sub-bottom profiles along transect 4. **(a)** The full extent of transect 4 as shown in Figs. 1 and 4. The location of the crossing profile on which the core 4-PC1 site is located is marked by a black line. **(b)** Detail of the eastern side of the Herald Canyon transect 4. The identified reflectors R1–R5 discussed in the text are marked. **(c)** Division of acoustic units based on the identified reflectors in panel **(b)**.

TWT (two-way travel time) thick ( $\sim 41$  m, using a sound speed of  $1500 \text{ m s}^{-1}$ ) and comprised of a partly acoustically well-stratified upper unit underlain by an acoustically chaotic lower unit (Fig. 5b). These two units are separated by reflector R2, defined in shallower areas and traced to deeper depths. Reflectors R3 and R4 reveal that the sedimentation above reflector R2 on the eastern side of Herald Canyon is characterized by onlapping, commonly interpreted to represent sea level transgression (Fig. 5c). Reflector R5 is defined to constrain an upper acoustically well-stratified subunit within the sediment accumulated above R2, reaching a maximum thickness of about 12 ms TWT ( $\sim 9$  m,  $1500 \text{ m s}^{-1}$ ; Fig. 5b).

### 3.2 Sediment stratigraphy

The physical and chemical sediment properties of cores 2-PC1 and 4-PC1 are shown in Fig. 3. Core 2-PC1 is defined by a single lithologic unit (unit A) consisting of gray to olive-gray clay. Some sections are dark to very dark gray in color with occasional mottling. The measured density, magnetic susceptibility and stable carbon isotopes of core 2-PC1 are relatively stable throughout the entire core. Density gradually decreases toward the top with values up to around  $1.2 \text{ g cm}^{-3}$  in the lower part of the core to  $1.1 \text{ g cm}^{-3}$  in its upper section. The  $\delta^{13}\text{C}_{\text{org}}$  values show a slight gradual upward increase from  $-22.5\text{‰}$  in the base of the core to  $-22\text{‰}$  in its upper part. The uppermost  $\sim 40$  cm of the core, however, shows a

decrease toward lower values. Core 4-PC1 is comprised of two major units (A and B) with the lowermost unit subdivided into B<sub>1</sub> and B<sub>2</sub>. Unit A consists of a similar lithology as 2-PC1 regarding both composition and coloration. Units A and B are separated by a transition in sediment physical properties between 412 and 400 cm. Lithostratigraphically this transition is marked by a change from a more consolidated sandy clayey silt containing intervals of darker gray laminae to a gray or olive-gray clayey silt. It is captured in the high-resolution multi-sensor core logging data as a notable decrease in bulk density from generally > 1.6 g cm<sup>-3</sup> below 400 cm to < 1.4 g cm<sup>-3</sup> above 390 cm. Magnetic susceptibility generally follows the bulk density trend, although with greater internal variability, and contains a major shift from higher to lower susceptibility occurring at about 40 cm up core from where bulk density changes; i.e. the susceptibility change occurs within the upper section of the core characterized by lower  $\delta^{13}\text{C}_{\text{org}}$  values. Measured  $\delta^{13}\text{C}_{\text{org}}$  and weight % BSi show a remarkably similar trend, with  $\delta^{13}\text{C}_{\text{org}}$  around -25 and -22‰ in the lower and upper half, respectively, and biogenic silica concentrations increasing from around 0–1 % below 400 cm to approximately 15 % in the upper sediments. The transition in sedimentary regimes is defined by the base of the abrupt increase in  $\delta^{13}\text{C}_{\text{org}}$  values occurring between 412 and 402 cm, thus very similar to the observed change in sediment physical properties. The lower unit is subdivided into B<sub>1</sub> and B<sub>2</sub> by a further up-core decrease in magnetic susceptibility and bulk density between 503 and 513 cm. The undrained shear strength remains low (< 5 kPa) across the unit A–B<sub>1</sub> transition, but increases substantially below the B<sub>1</sub>–B<sub>2</sub> boundary, reaching a maximum of 32 kPa at 589 cm. The micropaleontological analysis of core 4-PC1 by Cronin et al. (2017) shows a much greater abundance of river-proximal and river-intermediate benthic foraminiferal species in the lower unit B than in the upper unit A. Up-core from the transition between units A and B at around 400 cm of core depth, the abundance of foraminiferal species indicating influences of river water remains low. Both benthic ostracod and foraminiferal assemblages are dominated by fully marine mid-water shelf species in the upper section of core 4-PC1, i.e. unit A.

### 3.3 Sediment accumulation rates

Radiocarbon dates in the lower section of core 4-PC1 are clustered around 11–12 cal ka BP (Table 1) and indicate high sediment accumulation rates. Based on  $\Delta R = 50 \pm 100$  years and extrapolation above the youngest date at 417 cm of depth, the  $1\sigma$  age range estimate of the midpoint (407 cm) within the transition in  $\delta^{13}\text{C}_{\text{org}}$  between 412 and 402 cm is 10 787–11 209 cal yr BP with a median age of 11 065 cal yr BP. This extrapolation was done using a Bayesian approach that accounts for all dated levels below the transition (Ramsey, 2009). In order to test the sensitivity of different  $\Delta R$  values, we also include scenarios with

$\Delta R = 300$  and 500 years. This yield extrapolated ages at 407 cm in core 4-PC1 of  $\sim 11.1$  cal ka BP for  $\Delta R = 50$  years,  $\sim 10.8$  cal ka BP for  $\Delta R = 300$  years and  $\sim 10.5$  cal ka BP for  $\Delta R = 500$  years (Fig. S1 in the Supplement). The upper 400 cm of the core ranges from the present day to approximately 8.5 cal ka BP based on a radiocarbon date at 399 cm just above the major transition. This implies a hiatus or very low sediment accumulation rates in the early to mid-Holocene and a return to higher rates in the last ca. 3000 years of  $\sim 112$  cm kyr<sup>-1</sup>. The upper section of core 4-PC1 overlaps the age range of the 820 cm long core 2-PC1 (Fig. 3; Pearce et al., 2017). Core 2-PC has an average sediment accumulation rate over the last 4000 years of  $\sim 200$  cm kyr<sup>-1</sup>, implying that sediment has accumulated at nearly double the rate on the shallow flanks of Herald Canyon compared to its deeper and more central section.

### 3.4 Core–seismic integration

The logged physical properties (bulk density and p-wave velocity) of core 4-PC1 were resampled from core depth to TWT using the measured velocity and displayed on the nearest chirp sonar sub-bottom profile (Fig. 6). This chirp profile is comprised of a crossing line to transect 4 (Fig. 5). The distance between the coring site and the nearest chirp profile is within the accuracy of GPS navigation, which is approximately  $\pm 10$  m. In other words, core 4-PC1 is considered to be located directly on the chirp profile as far as we can determine with the accuracy of our navigation. There is a peak in both sediment higher bulk density and p-wave velocity coinciding with the traced reflector R5 (Fig. 6). Although core 4-PC1 does not appear to penetrate all the way to reflector R2, marking the upper part of the acoustically chaotic unit, it remains possible that the higher shear strength and higher density sediments comprising subunit B<sub>2</sub> may have come from this acoustic unit. Importantly, the cored sequence between R2 and R5 is a condensed acoustic interval thickening toward the east. This is an observation that can explain the reduced sedimentation rate and/or hiatus seen in the core chronology across the unit A–B transition.

## 4 Discussion

For several decades the debate over how and when the first human migration into America took place has been intense (Barton et al., 2004). The main controversy has been whether or not the so-called Clovis hunters were the first to make it across the Bering Land Bridge to inhabit America or if there were earlier cultures that may have used other alternative pathways to the New World (Barton et al., 2004). The maximum age range for the first appearance of the Clovis culture in North America has been estimated at 13 110 to 12 660 cal yr BP from <sup>14</sup>C dating of archaeological finds (Waters and Stafford, 2007). This age range implies that the oldest proposed estimates for the reopening of the Bering

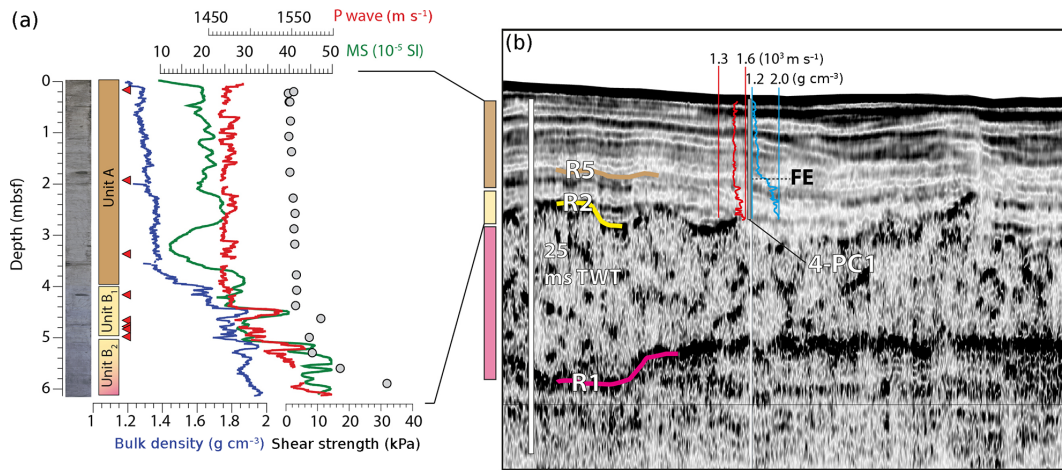


**Figure 6.** Core–seismic integration of 4-PC1. **(a)** Core image, interpreted lithologic units and sediment physical properties. Lithologic units are colored to match the interpreted seismic stratigraphy in Fig. 5. Uncertainty related to whether subunit B<sub>2</sub> penetrated reflector R2 is shown by faint pink shading. **(b)** Measured physical properties (p-wave velocity, bulk density) of core 4-PC1 overlaid on the chirp sonar profile crossing the coring site. The core depth is resampled to TWT using the measured p-wave velocity. FE marks the location in the core interpreted to represent the flooding event of the Bering Strait. Note that the location of the p-wave velocity and bulk density curves are slightly offset from the coring site (marked by a gray bar) for display purposes.

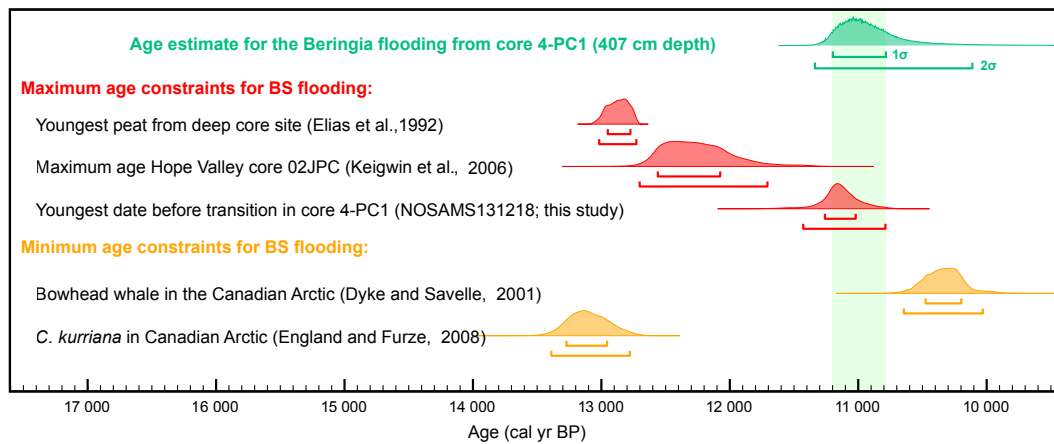


**Figure 7.** Published age estimates of the Bering Strait (BS) flooding compared with the age estimate from this work (green). The age estimates are divided into maximum (red) and minimum (yellow) age constraints. All ages and calibrations are listed in Table 1 and are shown here as calendar years BP (see text regarding the applied calibration of <sup>14</sup>C ages).

Strait overlap in time with the first signs of the Clovis culture (Fig. 7). Evidence of pre-Clovis cultures that made it into North and South America and the likelihood that they traveled by boat across the Bering Strait have toned down the significance of a Bering Land Bridge for human migration pathways (Erlandson et al., 2007). However, the paleogeography of the Bering Land Bridge provides key boundary conditions for both human and animal migration pathways that must be considered in parallel with the archaeological history of the first human settlements in America. In addition, the reconnection between the Pacific and the Arctic oceans through the Bering Strait has been suggested to influence the Holocene climate evolution that followed the last glaciation

(De Boer and Nof, 2004b; Hu et al., 2012; Ortiz et al., 2012; Shaffer and Bendtsen, 1994). The Bering Strait throughflow also provides one-third of the present-day freshwater input to the Arctic, and its associated heat transport controls the extent of the Arctic sea ice (Woodgate et al., 2012). Despite its relevance to several scientific questions, the time span for the Bering Land Bridge along with its paleogeography and environment is far from resolved due to the challenges associated with surveying Arctic marine areas and finding well-preserved datable material. Our study provides a new age constraint for the reopening of the Bering Strait and new insights into how the area of Herald Canyon developed geologically during the last deglaciation.

The seismic stratigraphy provides the broader spatial context for the two studied cores and helps us integrate the results of the detailed core studies when addressing the post-glacial development of the Bering Strait region. Reflector R1 identified in transect 4 marks an erosional unconformity and the base of Herald Canyon (Fig. 5b, c). This reflector does not merge with reflector R2, which we interpret to represent the land surface from the lower Last Glacial Maximum (LGM) and the Late Glacial sea level. The geological process behind the erosional unconformity marked by R1 most likely played a critical role in shaping the general morphology of Herald Canyon. While this unconformity appears similar to several ice-eroded surfaces mapped on the continental shelves, ridges and plateaus of the Arctic Ocean (Jakobsson et al., 2014), Herald Canyon is a much smaller and less pronounced physiographic feature than the smallest Arctic cross-shelf troughs formed by ice streams (Batchelor and Dowdeswell, 2014). However, with the relatively sparse geophysical mapping data it is not possible to completely rule out the possibility that glacial ice played some part in shaping the base of Herald Canyon. The Chukchi shelf northwest of the Alaskan coast contains several paleochannels and valleys (Hill and Driscoll, 2008). Most of these incisions, mapped more than 120 km east of our survey, are interpreted to have been formed during sea level falls associated with glacial periods, although some have been linked to increased meltwater drainage following the LGM (Hill and Driscoll, 2008). These channels indicate a flow east of Herald Canyon toward the shelf break. However, drainage from the Hope Valley area directly north of the Bering Strait is proposed to have taken the route toward Herald Canyon (McManus et al., 1983), which may provide an explanation for the underlying valley and the erosional unconformity represented by reflector R1 (Figs. 1, 4, 5).

Sediment accumulation along the eastern side of Herald Canyon atop reflector R2 is interpreted to represent a drift deposit influenced by the deglacial transgression, as indicated by the overlapping reflectors R3 and R4 (Fig. 5b, c). Reflector R5 may mark a subtle change in marine sedimentation and is traced all the way up to the shallower section of transect 4 (Fig. 5b, c). The core–seismic integration does not precisely relate this change in acoustic appearance to the change in sediment physical properties, specifically bulk density, measured in core 4-PC1 at about 400 cm down core. This is because R5 appears to be situated just below the upward decrease in both bulk density and p-wave velocity (Fig. 6), which implies that R5 is a good marker in the sub-bottom profiles preceding the major lithological transition at 400 cm down core. However, there is uncertainty in the core–seismic integration in that the resolution of the chirp sonar profiles is on the order of 70 cm with a 2.5–7 kHz pulse.

We interpret the transition in sediment physical and chemical properties in core 4-PC1 to mark the time when Pacific water began to enter the Arctic Ocean through the Bering Strait (Fig. 3). This transition in core 4-PC1 is dated

to  $\sim 11$  cal ka BP (median age 11 065 cal yr BP) based on a series of radiocarbon dates predating the shift and  $\Delta R$  of 50 years (Table 1; Figs. 3, 7). The inferred  $\Delta R$  value is a critical component for this age estimation; by applying higher  $\Delta R$  values, the age of the flooding moves progressively toward younger ages and thus further away from previously published age estimates (Figs. S1, 7). Moving up core from this level, measured  $\delta^{13}\text{C}_{\text{org}}$  values and BSi concentrations both increase to reach the modern values measured in the core tops. High BSi concentrations in the sediments are interpreted to show when biosilica-rich Pacific waters flowed through the Bering Strait. The high presence of biogenic silica, including diatoms, radiolaria, siliceous sponges and silicoflagellates, is a characteristic signature of Pacific waters today that has been used in oceanographic studies to trace advective patterns of Pacific waters in the Arctic Ocean (Anderson et al., 1983). Sediment bulk density commonly reflects the BSi content due to its lower grain density compared to quartz ( $2.65 \text{ g cm}^{-3}$ ),  $\sim 2.0 \text{ g cm}^{-3}$  for diatoms and sponges and  $\sim 1.7 \text{ g cm}^{-3}$  for radiolaria (DeMaster, 2003). In unit B of core 4-PC1, the preserved BSi is close to zero, suggesting a completely different depositional environment with no Pacific water inflow. A major change in sedimentary environment and water mass influence is similarly captured by changes in ostracod and benthic foraminiferal assemblages (Cronin et al., 2017). Furthermore, the higher  $\delta^{13}\text{C}_{\text{org}}$  values seen above the lithologic transition indicate a larger contribution from marine phytoplankton (Fischer, 1991; Mueller-Lupp et al., 2000). Taken together, the lithologic transition from unit B to A signifies a change from a near-shore environment with a terrestrial input of organic matter to a full marine continental shelf setting (Fig. 3). It should be emphasized that the estimated time for the flooding is based on maximum age constraints only, since the short transition interval may include a hiatus implied by the early Holocene date (8570 cal yr BP median age) at 399 cm of depth (Table 1; Fig. 7).

Estimations of the global eustatic sea level at 11 cal ka BP range between approximately 56 and 40 m below the present level (Lambeck et al., 2014; Peltier and Fairbanks, 2006; Fig. 2), which implies that the present sills in the Bering Strait separating the Arctic and Pacific oceans could potentially be flooded without considering local isostasy or post-glacial sediment deposition or erosion (Fig. 1). The global paleotopographic model ICE-6G\_C (Peltier et al., 2015) suggests that the land bridge between Asia and America still existed in the vicinity of the Bering Strait at 11.5 cal ka BP and was breached at about 11 cal ka BP (Fig. 8). Our timing of the flooding hence fits well with the paleotopography of ICE-6G\_C. The influence from glacial isostasy on the region near the Bering Strait is minor in ICE-6G\_C because this region was largely ice free during the LGM and served as a refugium for flora and fauna (Elias and Brigham-Grette, 2013).

Although an age estimate of 11 cal ka BP for the Bering Strait flooding is later than suggested in most other publica-

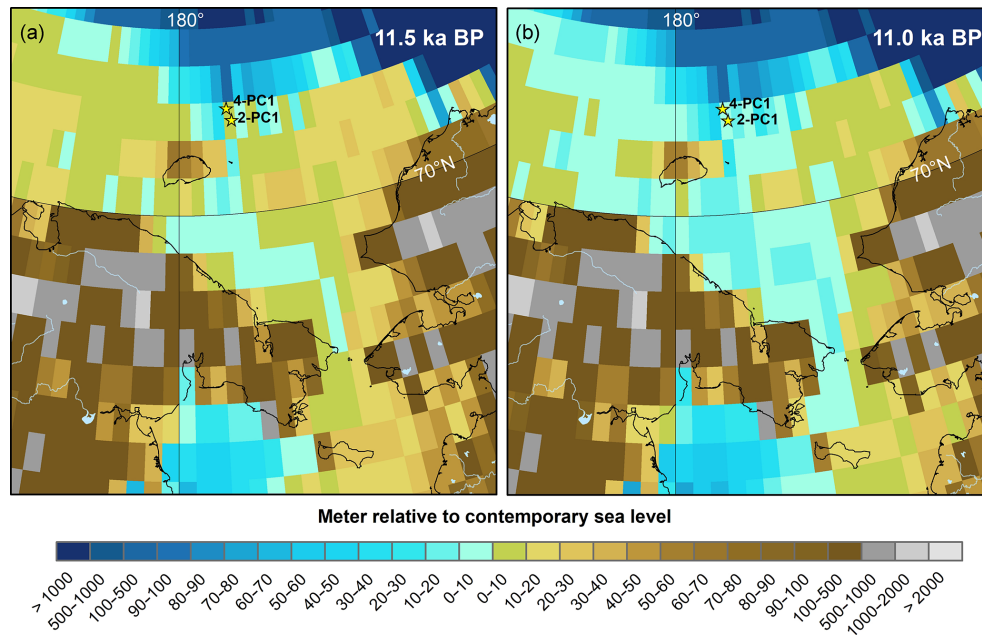


**Figure 8.** Paleotopography of the Beringia region based on the model ICE-6G\_C (Peltier et al., 2015) at 11.5 cal ka BP (a) and 11.0 cal ka BP (b). The Bering Strait is first flooded according to ICE-6G\_C at 11 ka BP, which is consistent with the age estimate in our study. The coring sites of 2-PC1 and 4-PC1 are shown as references. Blue indicates depths and green to brown indicates heights above sea level.

tions (Elias et al., 1996; England and Furze, 2008; Keigwin et al., 2006), it is compatible with nearly all data presented in these previous studies. No direct age determinations exist for the flooding, and existing age estimates are based on either maximum or minimum constraining ages. The age constraint provided by Elias et al. (1996) is based on identified peats underlying marine sediments in the Chukchi Sea. They dated the youngest peat from core 85–69 at 44 m of water depth (Fig. 1) to  $\sim 12.9$  cal ka BP (Table 1; Fig. 7). This indicates that by that time, the site was not yet flooded by the marine transgression, which is entirely consistent with our suggestion of an 11 cal ka BP Bering Strait flooding. Another maximum age constraint is obtained from core 02JPC from Hope Valley (Fig. 1), although this was originally presented as a minimum age for the flooding in Keigwin et al. (2006). Their study presented an abrupt change from a sandy layer containing terrestrial plant fragments to marine silt around 850 cm of depth in core 02JPC. Another rapid transition followed at 830 cm down core, consisting of a large turnover in stable isotopic composition of foraminifers (Keigwin et al., 2006). For the entire sequence, a single radiocarbon date is available, yielding a date of  $10900 \pm 140$   $^{14}\text{C}$  yr BP obtained from benthic foraminifers at 845.5 cm of depth in core 02JPC (Table 1, Fig. 7) thus derived from between the terrestrial sand and the isotopic change into fully marine conditions. Keigwin et al. (2006) assumed that the first marine waters to flood their core site in Hope Valley would have been sourced from the Bering Sea, and therefore the single ra-

diocarbon age provides a minimum age for the Bering Land Bridge flooding. The most recent high-resolution bathymetric dataset for the Chukchi Sea (ARDEM; Danielson, 2015), however, suggests that the initial flooding of Hope Valley with marine waters could instead have been sourced from the Arctic Ocean rather than the Pacific (Fig. 1). If the subsequent shift in isotopic composition in 02JPC then represents a rapid sea level rise and the Bering Strait flooding, the radiocarbon date precedes it and thus provides a maximum age constraint for the event. Similar to core 4-PC1 from Herald Canyon, we applied  $\Delta R = 50 \pm 100$  years for the calibration of this pre-flooding radiocarbon age, resulting in a calibrated age of around 12.5 cal ka BP (Table 1). This maximum age constraint for the Bering Land Bridge flooding is consistent with our estimate of 11 cal ka BP (Fig. 7). A minimum age for the opening of the strait is provided in Dyke and Savelle (2001), who dated the remains of bowhead whales in the Canadian Arctic Archipelago, which are assumed to originate from the Bering Sea; their appearance in the Arctic thus implies an open Bering Strait. The oldest age reported in this study is  $10210 \pm 70$   $^{14}\text{C}$  yr BP, which, using  $\Delta R = 740$  years for the region (McNeely et al., 2006), corresponds to ca. 10.5 cal ka BP (Table 1). Again, this age constraint is compatible with our flooding estimate of 11 cal ka BP (Fig. 7). The remaining age constraint on the flooding is the one given by England and Furze (2008), who used the appearance of the mollusc *Cyrtodaria kurriana* in Mercy Bay (Banks Island, Canadian Arctic Archipelago) as an indicator for an open

gateway to the Pacific. The minimum age constraint provided in this study is 11 500<sup>14</sup>C yr BP (Table 1), which, using the same  $\Delta R = 740$  years (McNeely et al., 2006), corresponds to ca. 13 cal ka BP (England and Furze, 2008). This age constraint for the Bering Land Bridge flooding predates our estimate by about 2000 years and is the only study incompatible with our findings (Fig. 7). This discrepancy would argue for an alternative explanation for the appearance of *Cyrtodaria kurriana* in Banks Island, other than a necessary connection to the Pacific Ocean through the Bering Strait. Several alternative mechanisms, such as migration along the North-east Passage, are discussed in England and Furze (2008) and could be further explored.

What are the broader scientific implications of a Bering Strait reopening at about 11 cal ka BP, rather than earlier, apart from the longer existence of a land pathway for human and animal migration between Asia and America, as suggested in previous studies? From a multitude of climate simulations and oceanographic analyses, an open Bering Strait is suggested to have an effect on climate stability (De Boer and Nof, 2004b; Ortiz et al., 2012; Sandal and Nof, 2008; Shaffer and Bendtsen, 1994). Most of these studies suggest that the Bering Strait throughflow influences the Atlantic Meridional Overturning Circulation (AMOC) because it allows greater freshwater export from the Arctic Ocean that influences the area of the North Atlantic where deep water is formed. By delaying the reopening of the Bering Strait to occur after the Younger Dryas stadial, its influence on climate must instead be sought in the early Holocene. The global temperature reconstruction by Marcott et al. (2013) shows a rapid warming of about 0.6° C from 11.3 cal ka BP to a warm plateau beginning at 9.5 cal ka BP. The mechanisms behind the rapid climate warming and oscillations in the early Holocene have been a subject of much discussion (Hoek and Bos, 2007), and with the reopening of the Bering Strait placed within this time period, new considerations may follow. Furthermore, the opening of the Bering Strait provides a transport route for Pacific surface water to the North Atlantic through the Arctic Ocean with potential implications for the ecosystem. Did this transport result in much higher nutrient concentrations in the Arctic Ocean and North Atlantic than before the opening? If so, the opening may well have boosted primary production and enhanced the productivity of higher trophic organisms, for instance along the North American eastern coast. Finally, we note that meltwater pulse 1b (MWP1b) between about 11.4 and 11.1 cal ka BP following the Younger Dryas overlaps in time with our 1  $\sigma$  age range (10 800–11 244 cal yr BP) for the reopening of the Bering Strait. While this event is not evident in many sea level records (Bard et al., 2010; Lambeck et al., 2014), it shows up as an approximate 15 m sea level rise in the Barbados coral reef record (Abdul et al., 2016; Cronin, 2012; Peltier and Fairbanks, 2006; Fig. 2). In the most recent sea level reconstruction by Abdul et al. (2016) based on Barbados reef crest coral *Acropora palmata*, MWP1b is seen as a 14 ± 2 m sea level rise, reaching 40 mm yr<sup>-1</sup>, be-

ginning at 11.45 ka BP and ending at 11.1 ka BP. However, it should be noted that this result has been questioned because the Barbados sea level record may have been affected by local tectonic movements throughout the Late Glacial period, and the living depth of the coral *A. palmata* may not be able to capture rapid sea level rises accurately (Bard et al., 2016). However, if there was a rapid sea level rise associated with MWP1b, it fits well in time with our age estimate of the post-glacial flooding of the Bering Land Bridge and a subsequent reestablishment of a Bering Strait throughflow, which in turn may have affected the AMOC by causing a greater amount of fresher water to be exported out of the Arctic Ocean.

## 5 Conclusions

Analyses of new geophysical and sediment records acquired from Herald Canyon northeast of Wrangel Island indicate that a swift change from a near-shore environment to a Pacific-influenced open marine setting occurred close to 11 cal ka BP in this area. This corresponds in time to meltwater pulse 1b (MWP1b). We interpret the observed change in environmental conditions in this part of the Arctic Ocean to be caused by a sudden flooding of the Bering Strait and the submergence of the Bering Land Bridge. From this point in time, a Pacific–Arctic water connection was reestablished after the last glaciation with consequences for the Arctic Ocean circulation, sea ice, ecology and potentially Earth's climate.

**Data availability.** The associated data have been uploaded to the Bolin Centre database at Stockholm university: <http://bolin.su.se/data/>.

Persistent links to the three main datasets used (first title of the dataset, then the persistent link):

- Marine sediment core data from Chukchi Sea, Arctic Ocean, core SWERUS-L2-2-PC1: <http://bolin.su.se/data/Jakobsson-2017>.
- Marine sediment core data from Chukchi Sea, Arctic Ocean, core SWERUS-L2-4-PC1: <http://bolin.su.se/data/Jakobsson-2017-2>.
- Sub-bottom profiling data from Herald Canyon, Chukchi Sea: <http://bolin.su.se/data/Jakobsson-2017-3>.

**The Supplement related to this article is available online at <https://doi.org/10.5194/cp-13-991-2017-supplement>.**

**Author contributions.** MJ and CP prepared the manuscript with input from all authors. MJ and MO analyzed the geophysical and petrophysical data. CP analyzed the sediment data and led the dating work.

**Competing interests.** The authors declare that they have no conflict of interest.

**Special issue statement.** This article is part of the special issue “Climate–carbon–cryosphere interactions in the East Siberian Arctic Ocean: past, present and future (TC/BG/CP/OS inter-journal SI)”. It does not belong to a conference.

**Acknowledgements.** We thank the supporting crew and captain of the IB *Oden* and acknowledge support from the Swedish Polar Research Secretariat. Many thanks to Carina Johansson and Heike Siegmund from the Department of Geological Sciences at Stockholm University for laboratory assistance. This research and expedition was supported by the Knut and Alice Wallenberg Foundation (KAW). Individual researchers received support from the Swedish Research Council (Leif G. Anderson 2013-5105, Martin Jakobsson and Helen Coxall 2012-1680, Matt O’Regan 2012-3091, Christian Stranne 2014-478), the US National Science Foundation (Larry A. Mayer PLR-1417789), the USGS (Thomas M. Cronin), the Russian Government (Igor Semiletov, grant no. 14.Z50.31.0012) and the Danish Council for Independent Research (Christof Pearce, grant no. DFF-4002-00098\_FNU). Any use of trade, firm or product names is for descriptive purposes only and does not imply endorsement by the US Government. Data presented in the paper were acquired during the SWERUS-C3 expedition in 2014 and are available through the Bolin Centre for Climate Research database: <http://bolin.su.se/data/>.

Edited by: Carlo Barbante

Reviewed by: Julie Brigham-Grette and two anonymous referees

## References

- Aagaard, K., Weingartner, T. J., Danielson, S. L., Woodgate, R. A., Johnson, G. C., and Whitley, T. E.: Some controls on flow and salinity in Bering Strait, *Geophys. Res. Lett.*, 33, L19602, <https://doi.org/10.1029/2006GL026612>, 2006.
- Abdul, N. A., Mortlock, R. A., Wright, J. D., and Fairbanks, R. G.: Younger Dryas sea level and meltwater pulse 1B recorded in Barbados reef crest coral *Acropora palmata*, *Paleoceanography*, 31, 330–344, <https://doi.org/10.1002/2015PA002847>, 2016.
- Anderson, L. G., Dyrssen, D. W., Jones, E. P., and Lowings, M. G.: Inputs and outputs of salt, fresh water, alkalinity, and silica in the Arctic Ocean, *Deep-Sea Res. Pt. I*, 30, 87–94, [https://doi.org/10.1016/0198-0149\(83\)90036-5](https://doi.org/10.1016/0198-0149(83)90036-5), 1983.
- Bard, E., Hamelin, B., and Delanghe-Sabatier, D.: Deglacial Meltwater Pulse 1B and Younger Dryas Sea Levels Revisited with Boreholes at Tahiti, *Science*, 327, 1235–1237, <https://doi.org/10.1126/science.1180557>, 2010.
- Bard, E., Hamelin, B., Deschamps, P., and Camoin, G.: Comment on “Younger Dryas sea level and meltwater pulse 1B recorded in Barbados reefal crest coral *Acropora palmata*” by N. A. Abdul et al., *Paleoceanography*, 31, 1603–1608, <https://doi.org/10.1002/2016PA002979>, 2016.
- Barton, C. M., Clark, G. A., Yesner, D. R., and Pearson, G. A.: The Settlement of the American Continents: A Multidisciplinary Approach to Human Biogeography, The University of Arizona Press, Tucson, 2004.
- Batchelor, C. L. and Dowdeswell, J. A.: The physiography of High Arctic cross-shelf troughs, *Quaternary Sci. Rev.*, 92, 68–69, 2014, <https://doi.org/10.1016/j.quascirev.2013.05.025>, 2014.
- Bauch, H. A., Mueller-Lupp, T., Taldenkova, E., Spielhagen, R. F., Kassens, H., Grootes, P. M., Thiede, J., Heinemeier, J., and Petryashov, V. V.: Chronology of the Holocene transgression at the North Siberian margin, *Global Planet. Change*, 31, 125–139, [https://doi.org/10.1016/S0921-8181\(01\)00116-3](https://doi.org/10.1016/S0921-8181(01)00116-3), 2001.
- Conley, D. J.: An interlaboratory comparison for the measurement of biogenic silica in sediments, *Mar. Chem.*, 63, 39–48, [https://doi.org/10.1016/S0304-4203\(98\)00049-8](https://doi.org/10.1016/S0304-4203(98)00049-8), 1998.
- Conley, D. J. and Schelske, C. L.: Biogenic Silica, in: *Biogenic Silica*, in: *Tracking Environmental Change Using Lake Sediments*, edited by: Smol, J. P., Birks, H. J. B., Last, W. M., Bradley, R. S., and Alverson, K., Springer Netherlands, 2002.
- Cronin, T. M.: Rapid sea-level rise, *Quaternary Sci. Rev.*, 56, 11–30, <https://doi.org/10.1016/j.quascirev.2012.08.021>, 2012.
- Cronin, T. M., O’Regan, M., Pearce, C., Gemery, L., Toomey, M., Semiletov, I., and Jakobsson, M.: Deglacial sea-level history of the East Siberian Sea Margin, *Clim. Past Discuss.*, <https://doi.org/10.5194/cp-2017-19>, in review, 2017.
- Danielson, S. L., Dobbins, E. L., Jakobsson, M., Johnson, M. A., Weingartner, T. J., Williams, W. J., and Zarayskaya, Y.: Sounding the northern seas, *EOS*, 96, <https://doi.org/10.1029/2015EO040975>, 2015.
- Danielson, S. L., Weingartner, T. J., Hedstrom, K. S., Aagaard, K., Woodgate, R., Curchitser, E., and Stabeno, P. J.: Coupled wind-forced controls of the Bering–Chukchi shelf circulation and the Bering Strait throughflow: Ekman transport, continental shelf waves, and variations of the Pacific–Arctic sea surface height gradient, *Prog. Oceanogr.*, 125, 40–61, <https://doi.org/10.1016/j.pocean.2014.04.006>, 2014.
- De Boer, A. M. and Nof, D.: The Bering Strait’s grip on the northern hemisphere climate, *Deep-Sea Res. Pt. I*, 51, 1347–1366, <https://doi.org/10.1016/j.dsr.2004.05.003>, 2004a.
- De Boer, A. M. and Nof, D.: The Exhaust Valve of the North Atlantic, *J. Climate*, 17, 417–422, [https://doi.org/10.1175/1520-0442\(2004\)017<0417:TEVOTN>2.0.CO;2](https://doi.org/10.1175/1520-0442(2004)017<0417:TEVOTN>2.0.CO;2), 2004b.
- DeMaster, D. J.: 7.04 – The Diagenesis of Biogenic Silica: Chemical Transformations Occurring in the Water Column, Seabed, and Crust A2 – Holland, Heinrich D., in: *Treatise on Geochemistry*, edited by: Turekian, K. K., Pergamon, Oxford, 2003.
- Dyke, A. S. and Savelle, J. M.: Holocene History of the Bering Sea Bowhead Whale (*Balaena mysticetus*) in Its Beaufort Sea Summer Grounds off Southwestern Victoria Island, Western Canadian Arctic, *Quatern. Res.*, 55, 371–379, <https://doi.org/10.1006/qres.2001.2228>, 2001.
- Elias, S. A. and Brigham-Grette, J.: GLACIATIONS – Late Pleistocene Glacial Events in Beringia, in: *Encyclopedia of Quaternary Science (Second Edition)*, Elsevier, Amsterdam, 2013.
- Elias, S. A., Short, S. K., Nelson, C. H., and Birks, H. H.: Life and times of the Bering land bridge, *Nature*, 382, 60–63, <https://doi.org/10.1038/382060a0>, 1996.
- Elias, S. A., Short, S. K., and Phillips, R. L.: Paleocology of late-glacial peats from the bering land bridge, Chukchi Sea shelf region, northwestern Alaska, *Quatern. Res.*, 38, 371–378, [https://doi.org/10.1016/0033-5894\(92\)90045-K](https://doi.org/10.1016/0033-5894(92)90045-K), 1992.

- England, J. H. and Furze, M. F. A.: New evidence from the western Canadian Arctic Archipelago for the re-submergence of Bering Strait, *Quatern. Res.*, 70, 60–67, <https://doi.org/10.1016/j.yqres.2008.03.001>, 2008.
- Erlandson, J. M., Graham, M. H., Bourque, B. J., Corbett, D., Estes, J. A., and Steneck, R. S.: The Kelp Highway Hypothesis: Marine Ecology, the Coastal Migration Theory, and the Peopling of the Americas, *The Journal of Island and Coastal Archaeology*, 2, 161–174, <https://doi.org/10.1080/15564890701628612>, 2007.
- Fairbanks, R. G.: A 17 000-year glacio-eustatic sea level record: influence of glacial melting rates on the Younger Dryas event and deep-ocean circulation, *Nature*, 342, 637–642, <https://doi.org/10.1038/342637a0>, 1989.
- Fischer, G.: Stable carbon isotope ratios of plankton carbon and sinking organic matter from the Atlantic sector of the Southern Ocean, *Mar. Chem.*, 35, 581–596, [https://doi.org/10.1016/S0304-4203\(09\)90044-5](https://doi.org/10.1016/S0304-4203(09)90044-5), 1991.
- Goebel, T., Waters, M. R., and Rourke, D. H.: The Late Pleistocene Dispersal of Modern Humans in the Americas, *Science*, 319, 1497–1502, <https://doi.org/10.1126/science.1153569>, 2008.
- Grebmeier, J. M.: Shifting Patterns of Life in the Pacific Arctic and Sub-Arctic Seas, *Annu. Rev. Mar. Sci.*, 4, 63–78, <https://doi.org/10.1146/annurev-marine-120710-100926>, 2011.
- Hill, J. C. and Driscoll, N. W.: Paleodrainage on the Chukchi shelf reveals sea level history and meltwater discharge, *Mar. Geol.*, 254, 129–151, <https://doi.org/10.1016/j.margeo.2008.05.018>, 2008.
- Hoek, W. Z. and Bos, J. A. A.: Early Holocene climate oscillations—causes and consequences, *Quaternary Sci. Rev.*, 26, 1901–1906, <https://doi.org/10.1016/j.quascirev.2007.06.008>, 2007.
- Hopkins, D. M.: The Cenozoic history of Beringia—A synthesis, in: *The Bering Land Bridge*, edited by: Hopkins, D. M., Stanford University Press, Stanford, California, 1967.
- Hu, A., Meehl, G. A., Han, W., Otto-Blietner, B., Abe-Ouchi, A., and Rosenbloom, N.: Effects of the Bering Strait closure on AMOC and global climate under different background climates, *Prog. Oceanogr.*, 132, 174–196, <https://doi.org/10.1016/j.pcean.2014.02.004>, 2015.
- Hu, A., Meehl, G. A., Han, W., Timmermann, A., Otto-Blietner, B., Liu, Z., Washington, W. M., Large, W., Abe-Ouchi, A., Kimoto, M., Lambeck, K., and Wu, B.: Role of the Bering Strait on the hysteresis of the ocean conveyor belt circulation and glacial climate stability, *P. Natl. Acad. Sci. USA*, 109, 6417–6422, <https://doi.org/10.1073/pnas.1116014109>, 2012.
- Hultén, E.: Outline of the history of arctic and boreal biota during the Quaternary Period: their evolution during and after the glacial period as indicated by the equiformal progressive areas of present plant species, *Bokförlags aktiebolaget Thule*, Stockholm, 1937.
- Jakobsson, M., Andreassen, K., Bjarnadóttir, L. R., Dove, D., Dowdeswell, J. A., England, J. H., Funder, S., Hogan, K., Ingólfsson, Ó., Jennings, A., Krog Larsen, N., Kirchner, N., Landvik, J. Y., Mayer, L., Mikkelsen, N., Möller, P., Niessen, F., Nilsson, J., O'Regan, M., Polyak, L., Nørgaard-Pedersen, N., and Stein, R.: Arctic Ocean glacial history, *Quaternary Sci. Rev.*, 92, 40–67, <https://doi.org/10.1016/j.quascirev.2013.07.033>, 2014.
- Keigwin, L. D., Donnelly, J. P., Cook, M. S., Driscoll, N. W., and Brigham-Grette, J.: Rapid sea-level rise and Holocene climate in the Chukchi Sea, *Geology*, 34, 861–864, <https://doi.org/10.1130/g22712.1>, 2006.
- Lambeck, K., Rouby, H., Purcell, A., Sun, Y., and Sambridge, M.: Sea level and global ice volumes from the Last Glacial Maximum to the Holocene, *P. Natl. Acad. Sci. USA*, 111, 15296–15303, <https://doi.org/10.1073/pnas.1411762111>, 2014.
- Marcott, S. A., Shakun, J. D., Clark, P. U., and Mix, A. C.: A Reconstruction of Regional and Global Temperature for the Past 11 300 Years, *Science*, 339, 1198–1202, <https://doi.org/10.1126/science.1228026>, 2013.
- McManus, D. A. and Creager, J. S.: Sea-level data for parts of the Bering-Chukchi shelves of Beringia from 19 000 to 10 000 14C yr B.P., *Quatern. Res.*, 21, 317–325, [https://doi.org/10.1016/0033-5894\(84\)90071-1](https://doi.org/10.1016/0033-5894(84)90071-1), 1984.
- McManus, D. A., Creager, J. S., Echols, R. J., and Holmes, M. L.: The Holocene transgression of the flank of Beringia: Chukchi valley to Chukchi estuary to Chukchi Sea, in: *Quaternary Coastlines and Marine Archaeology: Towards the Prehistory of Land Bridges and Continental Shelves*, edited by: Masters, P. M. and Flemming, N. C., Academic Press London, 1983.
- McNeely, R., Dyke, A. S., and R, S. J.: Canadian Marine Reservoir Ages, Preliminary Data Assessment, Ottawa, 1–3, 2006.
- Mueller-Lupp, T., Bauch, H. A., Erlenkeuser, H., Hefter, J., Kassens, H., and Thiede, J.: Changes in the deposition of terrestrial organic matter on the Laptev Sea shelf during the Holocene: evidence from stable carbon isotopes, *Int. J. Earth Sci.*, 89, 563–568, <https://doi.org/10.1007/s005310000128>, 2000.
- Ortiz, J. D., Nof, D., Polyak, L., St-Onge, G., Lisé-Pronovost, A., Naidu, S., Darby, D., and Brachfeld, S.: The Late Quaternary Flow through the Bering Strait Has Been Forced by the Southern Ocean Winds, *J. Phys. Oceanogr.*, 42, 2014–2029, <https://doi.org/10.1175/JPO-D-11-0167.1>, 2012.
- Pearce, C., Varhelyi, A., Wastegård, S., Muschitiello, F., Barrientos, N., O'Regan, M., Cronin, T. M., Gemery, L., Semiletov, I., Backman, J., and Jakobsson, M.: The 3.6 ka Aniakchak tephra in the Arctic Ocean: a constraint on the Holocene radiocarbon reservoir age in the Chukchi Sea, *Clim. Past*, 13, 303–316, <https://doi.org/10.5194/cp-13-303-2017>, 2017.
- Peltier, W. R., Argus, D. F., and Drummond, R.: Space geodesy constrains ice age terminal deglaciation: The global ICE-6G\_C (VM5a) model, *J. Geophys. Res.-Sol. Ea.*, 120, 2014JB011176, <https://doi.org/10.1002/2014JB011176>, 2015.
- Peltier, W. R. and Fairbanks, R. G.: Global glacial ice volume and Last Glacial Maximum duration from an extended Barbados sea level record, *Quaternary Sci. Rev.*, 25, 3322–3337, <https://doi.org/10.1016/j.quascirev.2006.04.010>, 2006.
- Pickart, R. S., Pratt, L. J., Torres, D. J., Whittledge, T. E., Proshutinsky, A. Y., Aagaard, K., Agnew, T. A., Moore, G. W. K., and Dail, H. J.: Evolution and dynamics of the flow through Herald Canyon in the western Chukchi Sea, *Deep-Sea Res. Pt. II*, 57, 5–26, <https://doi.org/10.1016/j.dsr2.2009.08.002>, 2010.
- Pisareva, M. N., Pickart, R. S., Spall, M. A., Nobre, C., Torres, D. J., Moore, G. W. K., and Whittledge, T. E.: Flow of Pacific water in the western Chukchi Sea: Results from the 2009 RUSALCA expedition, *Deep-Sea Res. Pt. I*, 105, 53–73, <https://doi.org/10.1016/j.dsr.2015.08.011>, 2015.
- Ramsey, C. B.: Bayesian analysis of radiocarbon dates, *Radiocarbon*, 51, 337–360, <https://doi.org/10.1017/S0033822200033865>, 2009.

- Reimer, P. J., Bard, E., Bayliss, A., Beck, J. W., Blackwell, P. G., Bronk Ramsey, C., Buck, C. E., Cheng, H., Edwards, R. L., Friedrich, M., Grootes, P. M., Guilderson, T. P., Hafliðason, H., Hajdas, I., Hatté, C., Heaton, T. J., Hoffmann, D. L., Hogg, A. G., Hughen, K. A., Kaiser, K. F., Kromer, B., Manning, S. W., Niu, M., Reimer, R. W., Richards, D. A., Scott, E. M., Southon, J. R., Staff, R. A., Turney, C. S. M., and van der Plicht, J.: IntCal13 and Marine13 radiocarbon age calibration curves 0–50 000 years cal BP, *Radiocarbon*, 55, 1869–1887, [https://doi.org/10.2458/azu\\_js\\_rc.55.16947](https://doi.org/10.2458/azu_js_rc.55.16947), 2013.
- Reimer, P. J. and Reimer, R. W.: A marine reservoir correction database and on-line interface, *Radiocarbon*, 43, 461–463, <https://doi.org/10.1017/S0033822200038339>, 2001.
- Sandal, C. and Nof, D.: The Collapse of the Bering Strait Ice Dam and the Abrupt Temperature Rise in the Beginning of the Holocene, *J. Phys. Oceanogr.*, 38, 1979–1991, <https://doi.org/10.1175/2008JPO3877.1>, 2008.
- Shaffer, G. and Bendtsen, J.: Role of the Bering Strait in controlling North Atlantic ocean circulation and climate, *Nature*, 367, 354–357, <https://doi.org/10.1038/367354a0>, 1994.
- Stigebrandt, A.: The North Pacific: a global-scale estuary, *J. Phys. Oceanogr.*, 14, 464–470, [https://doi.org/10.1175/1520-0485\(1984\)014<0464:TNPAGS>2.0.CO;2](https://doi.org/10.1175/1520-0485(1984)014<0464:TNPAGS>2.0.CO;2), 1984.
- Watanabe, E. and Hasumi, H.: Pacific Water Transport in the Western Arctic Ocean Simulated by an Eddy-Resolving Coupled Sea Ice–Ocean Model, *J. Phys. Oceanogr.*, 39, 2194–2211, <https://doi.org/10.1175/2009JPO4007.1>, 2009.
- Waters, M. R. and Stafford, T. W.: Redefining the Age of Clovis: Implications for the Peopling of the Americas, *Science*, 315, 1122–1126, <https://doi.org/10.1126/science.1137166>, 2007.
- Woodgate, R. A. and Aagaard, K.: Revising the Bering Strait freshwater flux into the Arctic Ocean, *Geophys. Res. Lett.*, 32, L02602, <https://doi.org/10.1029/2004GL021747>, 2005.
- Woodgate, R. A., Stafford, K. M., and Prahl, F. G.: A Synthesis of Year-Round Interdisciplinary Mooring Measurements in the Bering Strait (1990–2014) and the RUSALCA Years (2004–2011), *Oceanography*, 28, 46–67, <https://doi.org/10.5670/oceanog.2015.57>, 2015.
- Woodgate, R. A., Weingartner, T. J., and Lindsay, R.: Observed increases in Bering Strait oceanic fluxes from the Pacific to the Arctic from 2001 to 2011 and their impacts on the Arctic Ocean water column, *Geophys. Res. Lett.*, 39, L24603, <https://doi.org/10.1029/2012GL054092>, 2012.